Comparison of the Performances of Different Geared Brushless-DC Motor Drives for Electric Bicycles

Ewgenij Starschich
Fakultät für Elektrotechnik und Informationstechnik
RWTH Aachen, Aachen, Germany
ewgenij.starchisch@rwth-aachen.de

Annette Muetze
Dept. of Electrical and Computer Engineering
University of Wisconsin–Madison, Madison, WI 53706 USA
muetze@engr.wisc.edu

***Abstract*— In this paper, we compare the technical performance of geared brushless-dc motor electric bicycle drive systems with both self-control mode and hysteresis-band (direct torque) control, where the operating cycle profiles used are based on actual road tests. In most cases, for a given gear ratio, hysteresis-band (direct-torque) control gives a better efficiency than self-control mode. However, with self-control, higher gear ratios can be used to increase the drive efficiency, where a drive with hysteresis-band control could not deliver the torque-speed combinations required by the riding profile. Furthermore, the improvement of the efficiency with use of a high-speed instead of a high-torque motor with a larger gear ratio or of increased battery voltage is not very significant, but comes with much larger physical dimensions of the gear.**

***Index Terms*— Power-assisted bicycle, geared drive, efficiency, modeling, performance evaluation.**

I. Introduction

The market for electric motor powered bicycles has been growing fast during the last years. Such electric bicycles can be used for a large variety of purposes, including serving as a vehicle for police or law enforcers, a guide bike during races, and for leisurely rides and commuting (e.g. [1]–[8]). Common issues such as high cost and weight can be addressed by custom-designed bicycles for given contexts [8]. Drives for electric bicycles are required to produce a variety of different pairs of torque and speed, and of rate of change of torque at a given speed. In this paper, we compare the technical performances of different geared brushless-dc (BLDC) motor electric bicycle drive systems with self-control mode and direct torque control (DTC). To this aim, a model of a geared electric bicycle drive for both control methods has been developed and implemented into the commercially available software package MATLAB® Simulink®. A very unique characteristic of the model is that the operating cycle profiles used as input are based on actual road tests. Thereby, the results shall be both based on and illustrated with requirements most reasonable for the considered application.

We begin the paper with comments on the electric bicycle market with a special emphasis on the drive systems used on the European market to illustrate the starting point of our investigations (Section II). Then, we present the selected BLDC-motor model (Section III), the selection of the investigated BLDC-motor control techniques (Section IV), the model structure and implementation (Section VI), and the selection of the motor parameters (Section VII). Next, the riding profile simulations are described in general terms (Section VIII) and the results in terms of the technical performance of the investigated drives are presented (Section IX). At the end, conclusions are drawn (Section X).

II. Comments on The Electric Bicycle Market

A. General overview

The market for electric bicycles ("e-bikes") and pedelecs (bicycles which only add electrical power to the power produced by the rider, but cannot fully drive the bicycle) has grown very fast during the last years. Notably in China, the spread of electric bicycles and electric bicycle manufacturing companies is very high. On the European and Japanese markets, it is smaller than in China but higher than in the US or in any other market. When compared to the Chinese market, more advanced technology is used on the European and Japanese markets, because the customers are more interested in high-quality and "high-tech" bicycles and are also able (and willing) to spend more money on the product.

Most DC-motor drives for electric bicycles offered on the US market are direct drives. When compared with a geared drive, a direct drive is simpler and less costly, but the motor is larger (and thus heavier) to produce the required torque. Most drives with BLDC-motors include a gear.

Until some years ago, the electric bicycle and pedelecs market was dominated by mostly relatively small companies specialized in this technology. Today, many larger bicycle companies have included electric bicycles and especially pedelecs into their programs. The electrical parts of the bicycle are supplied from companies specialized in these products [9]–[12].

Concerning the battery technology, there is also a difference between the European and the Chinese market. On the Chinese market, lead-acid batteries are widely used because of their relatively low cost. On the European market, lead-acid batteries are not used by any of the larger companies, but Nickel Cadmium (NiCd), Lithium Ion (Li-Ion), and Nickel Metal Hydride (NiMh) batteries [12].

B. Motor selection – European market

According to our findings, the European market of electrical bicycle drives seems to be dominated by three companies which use three different technologies, all of them being geared:

1) Heinzman: brushed hub wheel motors, designed to be mounted on a fork bracket [13], [14].
2) Sanyo: BLDC-motors, designed to be mounted on a fork bracket [9].

1-4244-0743-5/07/$20.00 ©2007 IEEE

3) Panasonic: BLDC-motors, designed to be mounted at the bottom bracket [10].

The parts provided by these companies are then used by several manufacturers of electric bicycles and pedelecs (Table I).

TABLE I
MAIN ELECTRIC BICYCLE MOTORS AND MANUFACTURERS ON THE EUROPEAN MARKET

Part manufacturer	Heinzmann	Sanyo	Panasonic
Bicycle manufacturer	Estelle	Sachs	Trek
	Swizzbee	Giant	Flyer
	Hercules		Panasonic

III. BLDC-Motor Model

For the modeling of the BLDC-motor, we use the commercially available BLDC-motor model that is included in the PLECS®-Package of Plexim GmbH [15]. It is comparable to the one presented in [16]. Generally, the BLDC is represented by a three-phase equivalent circuit, where each phase consists of a stator resistance, self inductance, and a trapezoidal back-EMF voltage source in series. One of the crucial aspects in the simulation is the back-EMF waveform. In the PLECS®-model, for each phase, the back-EMF voltage is determined by a shape function and the mechanical rotor speed ω_{m}. The shape function itself is expressed as a Fourier series of the electrical rotor angle. The model additionally includes the cogging torque, which is again expressed as a Fourier series of the electrical rotor angle [17].

The input signals of the model are the three stator phase voltages and the mechanical load torque, the output signals are the mechanical rotor speed, electrical rotor position, electrical torque, and the three back-EMF voltages.

IV. Selection of the Investigated BLDC-Motor Control Techniques

A. Note on BLDC-torque ripple

With BLDC-motors, the inverter acts as an electronic commutator that receives switching command pulses from the absolute position sensor, usually consisting of three low-cost Hall sensors. Among the disadvantages of BLDC-machines are the torque ripples that are inherently associated with this type of machine, notably where accurate position control is required. Generally, four types of torque ripple can be distinguished [18], [19]. However, for electric bicycle applications, none of these are of concern, as the bicycle system has a relatively large inertia which acts as damper to the pulsating torque.

B. Self-control mode with buck-converter

In the self-control (SC) mode, the inverter acts only as commutator. The motor current and therefore the electrical torque of the BLDC-motor are controlled by variation of the DC-voltage with a buck-converter [18]. The buck-converter for changing the dc-link voltage is a standard converter. For electric bicycle applications, a highly dynamic buck converter is required to obtain a wide speed range.

C. PWM-motor control-mode

In the PWM-motor control-mode the inverter combines the functions of commutator and buck-converter. Depending on the switching order of the MOSFETs, four control strategies can be distinguished [18]: Q1-mode (unipolar), Q6-mode (unipolar), Q1Q6-mode (bipolar), and Q1Q6 alternate-mode (bipolar). For the details of these techniques we refer to the literature, such as [18]. In the work presented here, we restrain ourselves to the self-control mode, both because of its easier implementation and because comparison of the various PWM-control techniques would exceed the limits of this contribution. Those results shall be discussed in a later publication.

D. Hysteresis-band control

With hysteresis-band control, the current or torque is controlled directly. The feedback signal is compared to the reference signal in a comparator with a given amount of hysteresis and the driving transistor is turned off or on when the error exceeds the upper or falls below the lower limit of the hysteresis-band [20]. The different switching orders of the MOSFETs discussed for PWM-control (Section IV-C) can also be used with hysteresis regulators.

Three different hysteresis-band control strategies can be used for BLDC control: (i) conventional current control, (ii) current control with current shaping, and (iii) direct torque control (DTC). With DTC, a smaller torque ripple than with conventional current control and a better torque control than with current control with current shaping can be obtained [21]. (Yet, we do not consider this as a key factor with this application, see Section IV-A.)

Most of the commercially available motors for electric bicycles and pedelecs have a built-in torque sensor, so that torque calculation from current and voltage measurements is not required. With a built-in torque sensor, several advantages over the other techniques, and being the easiest to be implemented, DTC is therefore used in the further analysis.

V. Planetary Gear Train

The main parameter for describing a drive with a gear is the gear ratio i,

$$i = \frac{\omega_{\mathrm{in}}}{\omega_{\mathrm{out}}}, \tag{1}$$

where ω_{in} and ω_{out} are the gear input and output speeds respectively (here: mechanical speed of the motor shaft and wheel speed). Assuming an ideal gear, it is also

$$i = \frac{T_{\mathrm{out}}}{T_{\mathrm{in}}}, \tag{2}$$

with the gear input and output torques T_{in} and T_{out}.

The biggest advantage of planetary gears over conventional gears for light vehicle applications is the reduced weight and volume. This is achieved by the force distribution over three or five teeth instead of one tooth [22]. Other advantages are the high efficiency, especially at low torque levels, and the symmetrical construction that allow high gear ratios with one-stage and thus compact gears. The maximum speed range of the gear ratio is generally limited by centrifugal forces and

the efficiency drop at high speeds [22]. For the construction and possible configuration of the planetary gear, we refer to the literature, such as [23].

The gear efficiency η_{gear} depends on many factors like tooth friction and the efficiency of the bearings. A so-called "rest efficiency" can be used as approximation for the first-cut gear design [24]:

$$\eta_{\text{gear}} = -\frac{1 - i \cdot (0.99)^2 \cdot 0.995}{i} \tag{3}$$

VI. Model Structure and Implementation

A. Overview

For the analysis of the technical performance of the different drives, a longitudinal dynamic model is required. For the analysis discussed in this paper, a "single-wheel model" [25] is used. In the "single-wheel model," the entire vehicle is described as a rotating mass. The model does not consider the road condition, motor placement, and bicycle form. For more advanced analysis of the bicycle dynamics, a more complex model, such as the one based on road-tire interactions would be required [26].

A module-based approach of the modeling of the overall system is taken. The model is implemented using the commercially available software package MATLAB® Simulink®. The three sub-modules that each consist of further sub-modules are the motor and inverter module (including the converter), the controller module, and the gear module. The individual modules can be exchanged to analyze the different combinations of motor, gear, control strategy, and battery voltage. A sketch of the overall model structure is shown in Figure 1. Exemplarily, Figure 2 shows the MATLAB® Simulink® implementation for self-control mode.

B. Motor

The PLECS® BLDC-model (Section III) is used as core of the motor module. If used as provided, the model includes the mechanical equation, has the load torque that acts on the shaft as input parameter, and computes the motor speed. However, when the overall model is extended to include the mechanical equation and the gear, as in the work reported here, the motor speed becomes the new input parameter. The motor speed is then calculated from the "single-wheel model" of the bicycle including the gear ratio i via an extra module (Section VI-E).

C. Inverter module

For both control strategies, self-control and hysteresis-band (DTC), this module includes an ideal voltage source, a resistance, which represents the battery internal resistance, the dc-link capacitor, and the inverter. The inverter is build from six ideal MOSFETs which receive the switching signals from the controller module. For the self-control mode, it also includes a buck-converter consisting of an ideal MOSFET, a diode and an inductor.

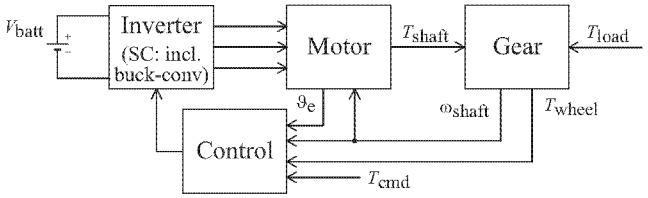

Fig. 1. Sketch of the overall model including inverter, motor, gear, and controller, including the mechanical equation.

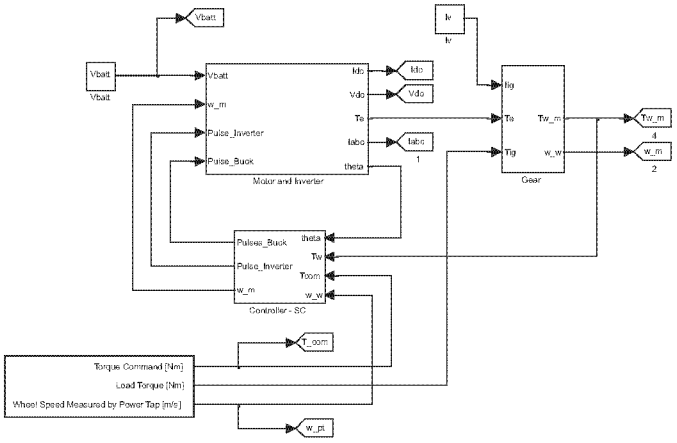

Fig. 2. MATLAB® Simulink® implementation of the model (self-control mode).

D. Controller module

For both control strategies, the flat area of the back-EMF (rotor position) is determined from the continuously increasing mechanical rotor angle. The controller determines the switching signals so that the current is in phase with the back-EMF flat area to obtain maximal torque and power. Furthermore, the switching signals are also used to control the current magnitude in a way that depends on the control method (Section IV).

In self-control mode, the duty cycle and therefore the output voltage of the buck-converter, which is the dc-link voltage of the inverter, is regulated by a PI-controller which operates on the torque error. The switching signals for the converter are generated with PWM, using Q1Q6-mode. In this configuration, the PI-controller directly influences the duty cycle of the buck-converter.

With respect to the hysteresis-band control, the torque band was set to $\Delta T = 0.4$Nm. This band was chosen to obtain a torque ripple comparable to the torque ripple seen with self-control mode and PWM-control (Note that the motor only sees the torque band converted with the gear ratio.), as obtained from preliminary studies. The switching order of the MOSFETS (unipolar, bipolar) influences the stress and the losses of the MOSFETs. Since ideal MOSFETs were selected for the simulation, the switching order does not influence the results of the simulations reported on here, the Q1-mode was implemented.

E. Gear module

For the simulation of the gear, a simplified gear model is used, assuming ideal gears, and neglecting the backlash, stiffness, and the viscous damper. These parameters can be neglected, because the mechanical dynamic accuracy of the motor is not very important for bicycles. The mechanical equation is applied to the torques, speeds, and inertias of the members of the planetary gear, the bicycle (single-wheel model) and the motor. For the purpose of straightforwardness, we do not elaborate on these derivations but refer to the literature [22], [25].

VII. Motor Parameter Selection

For the analysis, two different motors are selected. Considering the power supply of the bicycle given by the batteries, both motors are selected for an input voltage of 24V (Table II):

1) A "high-torque motor" (HT-motor) [28] which has output parameters comparable to commercially available bicycle motors.
2) A "high-speed motor" (HS-motor) [29] that has only approximately one third of the torque of the HT-motor but approximately 2.2 times higher speed.

TABLE II
PARAMETERS OF THE MOTORS USED IN THE SIMULATIONS

Peak torque	[Nm]	2.3	7.6
Rated torque	[Nm]	0.42	1.33
Rated speed	[rpm]	7400	3300
Rated power	[W]	328	459
Back-EMF constant	[V/rad/s]	0.0148	0.0325
Stator resistance	[Ω]	0.0345	0.0345
Stator inductance	[mH]	0.0645	0.1
Input voltage	[V]	24	24
Rated current	[A]	16.4	23
Friction torque	[Nm]	$7.5{\cdot}10^{-4}$	$7.5{\cdot}10^{-4}$
Rotor inertia	[Nm/s^2]	$42.3{\cdot}10^{-6}$	$12.7{\cdot}10^{-6}$
No. of poles		8	8

VIII. Riding Profile Simulations

A. Measurements and processing of the riding profile data

Riding profiles obtained from actual road tests were used as input for the simulations. These had been obtained with a commercially available bicycle that was equipped with a Power Tap® hub [30] to directly measure the torque and speed at the hub of the rear wheel of the test bicycle.

The data required for the simulation are derived from these measurements as follows: The measured torque is taken as the command torque, T_{cmd}, and becomes an input to the controller. The acceleration is calculated from the measured speed difference between two samples and used for the calculation of the load torque, T_{load}. The load torque is approximated using the mechanical equation, converted with the gear ratio and becomes input to the gear model, T^*_{load}. The measured wheel speed, ω_{wheel}, converted into the shaft speed, ω_{shaft}, is used as input into the motor model (Figure 3). The last step is done to decouple the input on this module and thus any conclusions drawn on the motor requirements from possible inaccuracies in the simulated speed introduced by the simplified single-wheel model.

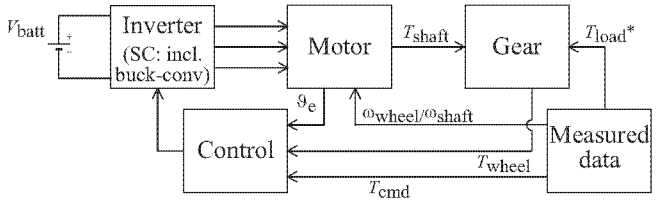

Fig. 3. Modified model of the drive system, data of measured riding profiles are used as input (compare with Figure 1).

B. Investigation of the drive performance

1) Comparison of simulated and measured data: An "ideal simulated wheel speed" can be obtained by applying the command torque to the gear model. However, because of the limitations given by the single wheel model, this speed does not follow the measured speed very well. We therefore take the following approach to verify if the command torque that is determined by the riding profile can be produced by the drive (Figure 4):

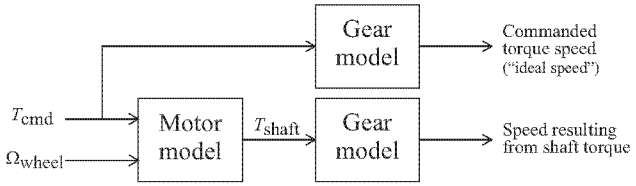

Fig. 4. Implementation of speed simulation and recording of simulated riding profile.

The "ideal commanded torque speed" is obtained as described above and is compared to the simulated wheel speed that is obtained from applying the torque actually produced by the motor to the gear model. If both are equal, the shaft torque of the motor equals the command torque and the drive can achieve the considered riding profile.

2) Energy calculations: $\tilde{\eta}$ and $\bar{\eta}$: The energy consumption during the bicycle ride is analyzed with different control and gear ratio configurations. The mechanical energy required for a given riding profile, W_{mech}, is calculated from the torque and speed at the wheel. The energy consumed by the drive during a given profile is calculated from the voltage and the current provided by the battery. From these values, the efficiencies of the drive configuration $\tilde{\eta}$ (with ideal inverter/buck-converter and gear) are calculated.

In a subsequent step, the gear efficiency is included in the calculations to give the efficiency of the drive $\bar{\eta} = \tilde{\eta} \cdot \eta_{\text{gear}}$, with the gear efficiency η_{gear} according to (3).

IX. Different Drive Configurations – Results

A. Overview of investigated configurations

Simulations with different combinations of control strategies and gear ratios are carried out, to investigate their performance for the given field of application. The first set of simulations was carried out on the first 50s of the measured riding profile. This part contains both positive and negative speed and torque

slopes. The whole riding profile of 932s is simulated with the preferred motor-control strategy combination.

An overview of the different investigated configurations is shown in Table III.

TABLE III

OVERVIEW OF INVESTIGATED CONFIGURATIONS

Self-control mode and with hysteresis-band control, $i = 20$				
HT-motor	self-control	$i = 20$	$V_b = 24$V	Figure 5
HT-motor	hysteresis-band	$i = 20$	$V_b = 24$V	·
Self-control mode and with hysteresis-band control, $i = 14$				
HT-motor	self-control	$i = 14$	$V_b = 24$V	Figure 6
HT-motor	hysteresis-band	$i = 14$	$V_b = 24$V	·
Self-control mode, different gear ratios				
HT-motor	self-control	$i = 14$	$V_b = 24$V	Figure 7
HT-motor	self-control	$i = 16$	$V_b = 24$V	·
HT-motor	self-control	$i = 18$	$V_b = 24$V	·
HT-motor	self-control	$i = 20$	$V_b = 24$V	·
HT-motor	self-control	$i = 22$	$V_b = 24$V	·
HT-motor	self-control	$i = 24$	$V_b = 24$V	·
Hysteresis-band control, different gear ratios				
HT-motor	hysteresis-band	$i = 14$	$V_b = 24$V	Figure 8
HT-motor	hysteresis-band	$i = 16$	$V_b = 24$V	·
HT-motor	hysteresis-band	$i = 18$	$V_b = 24$V	·
HT-motor	hysteresis-band	$i = 20$	$V_b = 24$V	·
36V battery voltage				
HT-motor	self-control	$i = 30$	$V_b = 36$V	Figure 9
HT-motor	self-control	$i = 32$	$V_b = 36$V	·
HT-motor	self-control	$i = 34$	$V_b = 36$V	·
HT-motor	self-control	$i = 36$	$V_b = 36$V	·
HT-motor	hysteresis-band	$i = 18$	$V_b = 36$V	·
High-speed motor				
HS-motor	self-control	$i = 40$	$V_b = 24$V	Figure 10
HS-motor	self-control	$i = 46$	$V_b = 24$V	·
HS-motor	hysteresis-band	$i = 20$	$V_b = 24$V	·
HS-motor	hysteresis-band	$i = 40$	$V_b = 24$V	·

B. Comparison between BLDC-motor in self-control mode and with hysteresis-band control

Figures 5 and 6 show the simulated speed for the HT-motor with gear ratios $i = 20$ and $i = 14$ in self-control mode (HT-SC-G20, HT-SC-G14) and with hysteresis-band control (HT-HB-G20, HT-HB-G14). With increasing speed (after 35s simulation time), the speed of the HT-HB-G20 drive cannot follow the "ideal command torque speed," any more and the drive cannot deliver the commanded torque any more. Thus, it cannot produce enough torque to accelerate, and the drive speed does not follow the command torque speed any longer. However, the HT-SB-20 drive is able to deliver the same simulated speed as the ideal command torque speed. In order to obtain the ideal command torque speed with hysteresis-band (DTC) control, a gear ratio of $i = 14$ is required.

The efficiency difference between both modes, self-control and hysteresis-band control, is less than 2%, both with ideal and with non-ideal gear. With $i = 14$ for both strategies, hysteresis-band control has the higher efficiency of 92.8% and 83.9% with ideal/non-ideal gear, respectively. However, this efficiency is still lower than the one of the drive in self-control mode with $i = 20$, which is 93.8% and 86.8% with ideal/non-ideal gear (Table IV).

C. Investigation of different gear ratios

As it was seen for the HT-motor with hysteresis-band (DTC) control and gear ratio $i = 20$, the simulated speed could not follow the ideal command torque speed, what signifies that the commanded torque could not be provided by the drive. In order to investigate which gear combinations can provide the required torque for the given motor, control strategy, and battery voltage, the riding profile is simulated with different gear ratios for both control modes. For self-control mode, gear ratios $i = 14, 16, 18, 20, 22, 24$ (Figure 7), and for hysteresis-band control (DTC) gear ratios $i = 14, 16, 18, 20$ (Figure 8) are analyzed.

With self-control mode, gear combinations up to $i = 20$ can be used for the given riding profile. With $i = 24$, the speed drops rapidly after 38s riding time, illustrating well that the torque limit of the machine for the speed measured at this time moment is reached. With hysteresis-band control, the maximum gear ratio at which the riding profile can be followed is $i = 14$. Thus, with hysteresis-band control, the motor will operate at lower speeds than with self-control mode to obtain the same riding profile.

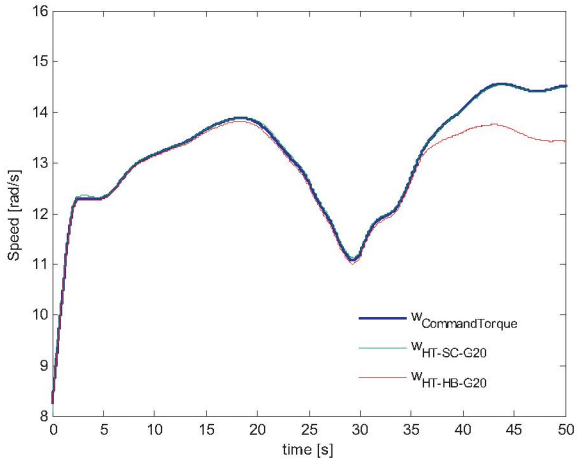

Fig. 5. Speed simulation comparison of HT-motor with gear ratio $i = 20$ in self-control mode (HT-SC-G20) and with hysteresis-band control (HT-HB-G20).

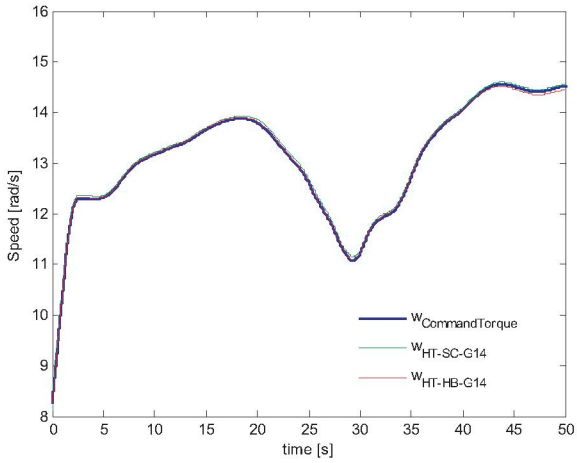

Fig. 6. Speed simulation comparison of HT-motor with gear ratio $i = 14$ in self-control mode (HT-SC-G14) and with hysteresis-band control (HT-HB-G14).

TABLE IV

ENERGY CONSUMPTIONS AND EFFICIENCIES; SIMULATION RESULTS, IDEAL GEAR, 50S RIDING PROFILE, $W_{MECH} = 1.088$WH, $\tilde{\eta}$: DRIVE EFFICIENCY WITH IDEAL GEAR, $\bar{\eta}$: DRIVE EFFICIENCY WITH NON-IDEAL GEAR

Drive	W_{cons}	$\tilde{\eta}$	η_{gear}	$\bar{\eta}$
HT-SC-G14	1.191Wh	91.4%	90.4%	82.6%
HT-SC-G16	1.172Wh	92.8%	91.3%	84.7%
HT-SC-G18	1.171Wh	92.9%	92.0%	85.4%
HT-SC-G20	1.160Wh	93.8%	92.5%	86.8%
HT-HB-G14	1.172Wh	92.8%	90.4%	83.9%
HT-HB-G16	1.149Wh	94.7%	91.3%	86.4%
HT-SC-G18-V36	1.162Wh	93.6%	92.0%	86.1%
HT-SC-G20-V36	1.160Wh	93.8%	92.5%	86.8%
HT-SC-G22-V36	1.156Wh	94.1%	93.0%	87.5%
HT-SC-G24-V36	1.152Wh	94.4%	93.4%	88.2%
HT-SC-G26-V36	1.150Wh	94.6%	93.7%	88.6%
HT-SC-G28-V36	1.150Wh	94.6%	93.9%	88.9%
HT-SC-G30-V36	1.149Wh	94.7%	94.2%	89.2%
HT-SC-G32-V36	1.124Wh	96.8%	94.4%	91.4%
HT-HB-G18-V36	1.193Wh	91.2%	92.0%	83.9%
HS-SC-G38	1.169Wh	93.1%	94.9%	88.3%
HS-SC-G40	1.164Wh	93.5%	95.0%	88.3%
HS-SC-G42	1.160Wh	93.8%	95.1%	89.2%
HS-SC-G44	1.156Wh	94.1%	95.2%	89.6%
HS-SC-G46	1.152Wh	94.4%	95.3%	90.0%

With respect to the drive efficiencies, the energy consumptions decrease with both control strategies by 2%...3% with ideal, and by 3%...4% with non-ideal gear, when comparing the drives with the higher gear ratios, self-control $i = 20$ and hysteresis-band control $i = 16$ (which can hardly follow), to those with $i = 14$. For the same gear ratio, and in line with the previous findings, the energy consumption of the hysteresis-band control is 2% smaller than the one in self-control (Table IV).

D. Investigation of a higher battery voltage

As the maximum speed of the motor is limited by the back-EMF, a boost-converter or higher battery voltage is considered to increase the maximum speed. The simulations with 36V battery voltage instead of 24V are analyzed in self-control mode for different gear ratios and with hysteresis-band control for $i = 18$ (Figure 9).

The energy consumptions and efficiencies with higher battery voltage and different gear ratios are shown in Table IV. When the gear ratio is almost doubled from $i = 18$ up to $i = 32$ in self-control mode, the efficiency increases by 3% with ideal gear, and 5% with non-ideal gear. The higher gear ratio results in a significant increase of the physical dimensions of the gear, and it is questionable if this effort can be justified for the given application. Furthermore, the efficiency with hysteresis-band control, $i = 18$, and 36V battery voltage is approximately the same as with hysteresis-band control, $i = 14$, and 24V battery voltage.

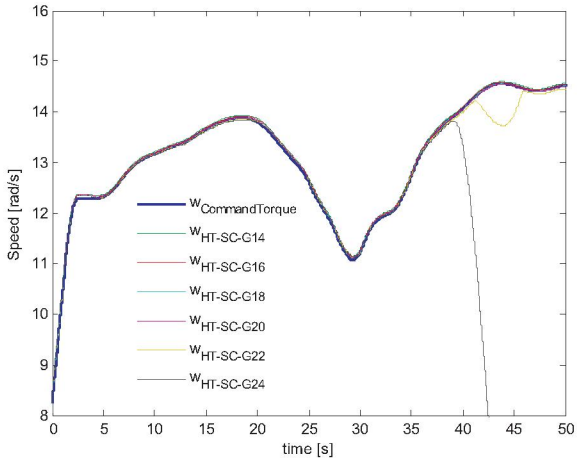

Fig. 7. Speed simulation of HT-motor in self-control mode (HT-SC-) and with gear ratios $i = 14...24$ (-Gxx).

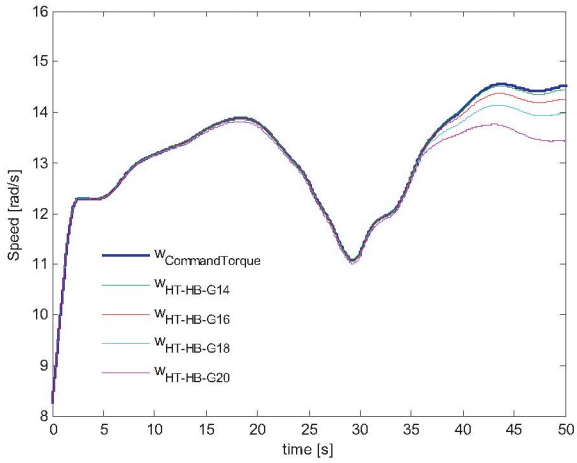

Fig. 8. Speed simulation of HT-motor with hysteresis-band control (HT-HB-) and with gear ratios $i = 14...20$ (-Gxx).

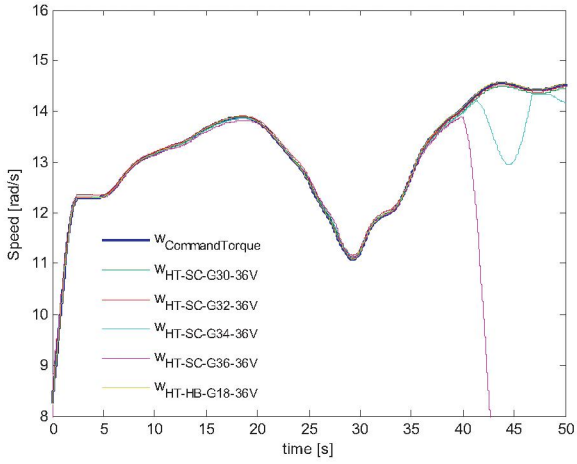

Fig. 9. Speed simulation with 36V battery voltage of the HT-motor in self-control mode (HT-SC-Gxx-36V) with gear ratios $i = 30...36$ (-Gxx-) and with hysteresis-band control and gear ratio $i = 18$ (HT-HB-G18-36V).

E. Analysis of the high-speed motor

The HS-motor with a higher gear ratio is analyzed and compared to the HT-motor (Section VII). Both self-control mode and hysteresis-band control are investigated with different gear ratios (Figure 10).

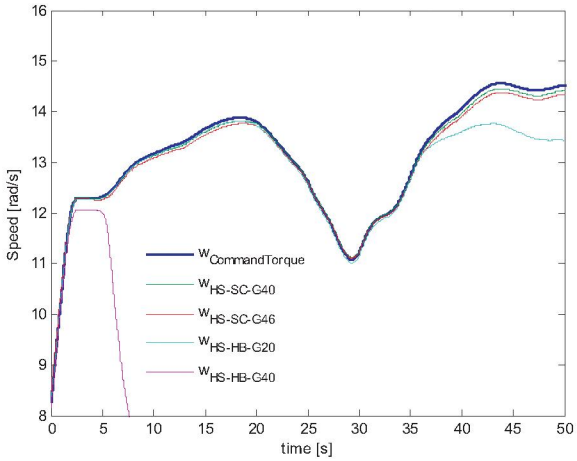

Fig. 10. Speed simulation with HS-motor in self-control mode (HS-SC-) with gear ratios $i = 40, 46$ (-Gxx) and with hysteresis-band control (HS-HB-) and gear ratios $i = 20, 40$ (-Gxx).

With self-control mode, the simulated speed follows the reference speed very well, even for gear ratios as high as $i = 46$. However, with hysteresis-band control, the simulated motor speed cannot follow the ideal torque command speed even for a low gear ratio of $i = 20$.

With respect to the efficiency, and considering again the larger physical sizes of a gear with larger gear ratio, the HS-motor in self-control mode does not show significant advantages when compared to the HT-motor: The difference between the efficiencies of the HT-motor with $i = 20$ and the HS-motor with $i \leq 46$ is less than 1% with ideal gear, and 3% with non-ideal gear (Table IV).

F. Simulation of a complete ride

Figure 11 shows the simulation of the complete ride of 932s with the HT-motor in self-control mode and gear ratio $i = 12$. This gear ratio is required so that the simulated speed, as produced by the drive, can follow the ideal torque command speed over the whole riding profile.

The mechanical energy required for the whole riding profile is $W_{\text{mech}} = 17.56\text{Wh}$ and the energy consumption of the drive is $W_{\text{cons}} = 20.10\text{Wh}$. Thus, the drive efficiency is $\tilde{\eta} = 87.4\%$ with ideal gear, and $\bar{\eta} = 77.9\%$ with non-ideal gear and $\eta_{\text{gear}} = 89.2$, according to (3). These results complete the overall picture that the efficiency decreases with a smaller gear ratios, but a larger operating area can be achieved.

X. Conclusions

The technical performances of different geared brushless-dc motor electric bicycle drive systems in self-control mode

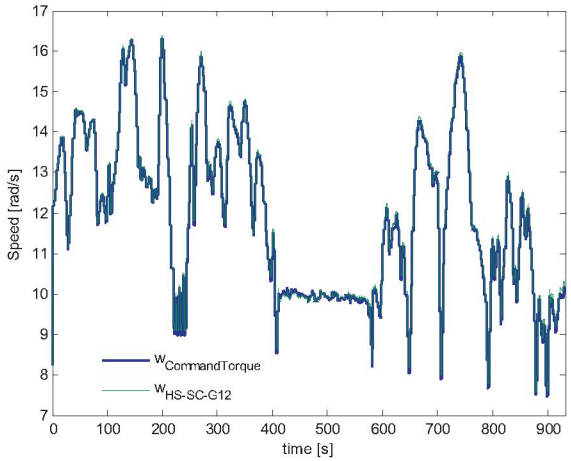

Fig. 11. Simulation of a complete ride of 932s with HT-motor in self-control mode and gear ratio $i = 12$ (HT-SC-G12).

with buck-converter, and with hysteresis-band control (DTC) have been compared. The comparison is based on riding profiles that are based on actual road tests. For a given gear ratio, hysteresis-band control gives a better efficiency than self-control mode, next to requiring less power electronic components. (Full PWM motor control shall be discussed in a later publication.) The disadvantage of hysteresis-band control when compared to self-control mode is that a smaller gear ratio has to be used for a given riding profile what reduces the maximum provided torque and thereby restricts the area the drive can operate in. Furthermore, the improvement of the efficiency with use of a high-speed instead of a high-torque motor with a larger gear ratio or of increased battery voltage is not very significant, but comes with much larger physical dimensions of the gear.

In future work, the model can be extended to include a better simulation of the battery system, non-ideal switches, and additional control of the output power as a function of the human power, as it is the requirement with pedelec-type electric bicycles.

Appendix

Appendix A: List of abbreviations

Acronym	Definition
DC	Direct Current
BLDC	Brushless DC
DTC	Direct Torque Control
EMF	Electromagnetic Force
HB	Hysteresis-band
HS-motor	High-Speed motor
HT-motor	High-Torque motor
PWM	Pulse-Width Modulation
SC	Self-control

Appendix B: List of symbols

Name	Description
i	gear ratio
T_{cmd}	command torque
T_{in}	input torque (gear)
T_{load}	load torque
T^*_{load}	load torque at gear side
T_{shaft}	shaft torque
T_{out}	output torque (gear)
T_{wheel}	torque at wheel
V_{batt}	battery voltage
W_{mech}	mechanical energy
ϑ_{e}	rotor angle (electric degrees)
η_{gear}	gear efficiency
$\tilde{\eta}$	drive efficiency with ideal gear
$\bar{\eta}$	drive efficiency with non-ideal gear
ω_{in}	input speed (gear)
ω_{out}	output speed (gear)
ω_{shaft}	shaft speed
ω_{wheel}	wheel speed

REFERENCES

[1] B. Kumar and H. Oman, "Power control for battery-electric bicycles," *Proceedings of NAECON '93 - National Aerospace and Electronics Conference*, vol. 1, pp. 428-434, Dayton, OH, May 24-28, 1993.

[2] W.C. Morchin, "Battery-powered electric bicycles," *Proceedings of Northcon '94*, pp. 269-274, Seattle, WA, October 11-13, 1994.

[3] E.A. Lomonova, A.J.A. Vandenput, J. Rubacek, B. d'Herripon, and G. Roovers, "Development of an improved electrically assisted bicycle," *Proceedings of 37th IEEE IAS Annual Meeting*, pp. 384-389, Pittsburgh, PA, October 13-18, 2002.

[4] F.E. Jamerson, *Electric bikes worldwide 2002: with electric scooters & neighborhood EVs*, Naples, Fla: Electric Battery Bicycle Co, 2002.

[5] A. Muetze, A.G. Jack, and B.C. Mecrow, "Brushless-dc motor using soft magnetic composites as a direct drive in an electric bicycle," *Proceedings of the 9th European Conference on Power Electronics and Applications (EPE), paper no. 350, Graz, 2001.*

[6] D.G. Wilson, J. Papadopoulos, and F.R. Whitt, *Bicycling science*, Cambridge, Mass: MIT Press, 2004.

[7] P. Fairley, "China's cyclists take charge: electric bicycles are selling by the millions despite efforts to ban them," *IEEE Sprectrum*, vol. 42, no. 6, pp. 54-69, June 2005.

[8] A. Muetze and Y.C. Tan, "Performance evaluation of electric bicylces," *Proceedings of 40th IEEE IAS Annual Meeting*, pp. 2865-2872, Hong Kong, October 2-6, 2005.

[9] SANYO Electric Co., Ltd., "SANYO – SANYO Electric Co., Ltd.," leaflet, available at http://www.jbpi.or.jp/english/jbg.html, accessed October 14, 2006.

[10] Panasonic Cycle Technology Co., Ltd., http://www.panabyc.co.jp/en/product_du.htm, accessed October 14, 2006.

[11] Sachs, "Sachs-Bikes: E-Bikes," http://www.sachs-bikes.de/produkte.php? marken_id=1&prod_cat=5, accessed October 14 2006.

[12] NewRide, "Fahrzeugkatalog 2006," available at http://www.newride.ch, accessed October 14, 2006.

[13] http://www.kinetics-online.co.uk/html/heinzmann_kits.shtml, accessed October 14, 2006.

[14] http://www.heinzmann.com/index.php?option=com_content&task=view&id=30&Itemid=128&lang=en, accessed October 14, 2006.

[15] Plexim GmbH, http://www.plexim.com, accessed October 14, 2006.

[16] P. Pillay and R. Krishnan, "Modeling, simulation, and analysis of permanent-magnet motordrives. II. The brushless DC motor drive," *IEEE Transactions on Industry Applications*, vol. 25, no. 2, March/April 1989.

[17] Plexim, "PLECS User Manual," available at http://www.plexim.com/downloads/plecs_documentation.html, accessed October 14, 2006.

[18] B.K. Bose, *Modern Power Electronics and AC Drives*, Prentice Hall, 2002.

[19] H. Zeroug, B. Boukais, and H. Sahraoui, "Analysis of torque ripple in a BDCM," *IEEE Transactions on Magnetics*, vol. 38, no. 2, pp. 1293-1296, 2002.

[20] J.R. Hendershot and T. Miller, *Design of brushless permanent-magnet motors*, 1994.

[21] Z.Q. Zhu, Y. Liu, and D. Howe, "Comparison of performance of brushless DC drives under direct torque control and PWM current control," *Proceedings of 8th International Conference on Electrical Machines and Systems* (ICEMS), vol. 2, pp. 1486-1491, Nanjing, P.R. China, September 27-29, 2005.

[22] P.W. Gold, *Maschinenelemente, Vorlesungsumdruck Band II* [Machine elements, course notes volume II; in German], (Institute for Machine Elements and Design, RWTH Aachen), 2003.

[23] R. Trautschold, *Standard Gear Book*, 1935.

[24] VDI, *VDI-Richtlinie: VDI 2157 Planetengetriebe; Begriffe, Symbole, Berechnungsgrundlagen* [VDI-Guideline: VDI 2157 Planetary gears; terms, symbols, calculation], 1978.

[25] P. Waltermann, "Modelling and control of the longitudinal and lateral dynamics of a series hybrid vehicle," *Proceedings of IEEE International Conference on Control Applications*, pp. 191-198, Dearborn, MI, September 15-18, 1996.

[26] L. Li, F.Y. Wang, and Q. Zhou, "Integrated longitudinal and lateral tire/road friction modeling and monitoring for vehicle motion control;" *IEEE Transactions on Intelligent Transportation Systems*, vol. 7, no. 1, pp. 1-19, March 2006.

[27] Moog Components Group, "Silencer Series Brushless DC Motors Commercial and Industrial," http://www.polysci.com/Motors/silencer.html, accessed October 14, 2006.

[28] Moog Components Group, motor BN34-45AF-01, in [27].

[29] Moog Components Group, motor BN34-25AF-01, in [27].

[30] Power Tap® is by Graber Products, Inc., 5253 Verona Road, Madison, WI USA, http://www.cycle-ops.com.